The tumbling spin state of (99942) Apophis

P. Pravec [a], P. Scheirich [a], J. Ďurech [b], J. Pollock [c], P. Kušnirák [a], K. Hornoch [a], A. Galád [a], D. Vokrouhlický [b], A.W. Harris [d], E. Jehin [e], J. Manfroid [e], C. Opitom [e], M. Gillon [e], F. Colas [g], J. Oey [h], J. Vraštil [a,b], D. Reichart [f], K. Ivarsen [f], J. Haislip [f], A. LaCluyze [f]

[a] *Astronomical Institute, Academy of Sciences of the Czech Republic, Fričova 1, CZ-25165 Ondřejov, Czech Republic*

[b] *Institute of Astronomy, Faculty of Mathematics and Physics, Charles University, Prague, V Holešovičkách 2, CZ-18000 Prague 8, Czech Republic*

[c] *Physics and Astronomy Department, Appalachian State University, Boone, NC 28608, U.S.A.*

[d] *MoreData! Inc., 4603 Orange Knoll Avenue, La Cañada, CA 91011, U.S.A.*

[e] *Institut d'Astrophysique de l'Université de Liège, Alle du 6 Aout 17, B-4000 Liège, Belgium*

[f] *Physics and Astronomy Department, University of North Carolina, Chapel Hill, NC 27514, U.S.A.*

[g] *IMCCE-CNRS-Observatoire de Paris, 77 avenue Denfert Rochereau, 75014 Paris, France*

[h] *Leura Observatory, Leura, N.S.W., Australia*

2013 November 26

Proposed running head: Apophis tumbling

Editorial correspondence to:
Dr. Petr Pravec
Astronomical Institute AS CR
Fričova 1
Ondřejov
CZ-25165
Czech Republic
Phone: 00420-323-620352
Fax: 00420-323-620263
E-mail address: ppravec@asu.cas.cz

Abstract

Our photometric observations of asteroid (99942) Apophis from December 2012 to April 2013 revealed it to be in a state of non-principal axis rotation (tumbling). We constructed its spin and shape model and found that it is in a moderately excited Short Axis Mode (SAM) state with a ratio of the rotational kinetic energy to the basic spin state energy $E/E_0 = 1.024 \pm 0.013$. (All quoted uncertainties correspond to 3σ.) The greatest and intermediate principal moments of inertia are nearly the same with $I_2/I_3 = 0.965^{+0.009}_{-0.015}$, but the smallest principal moment of inertia is substantially lower with $I_1/I_3 = 0.61^{+0.11}_{-0.08}$; the asteroid's dynamically equivalent ellipsoid is close to a prolate ellipsoid. The precession and rotation periods are $P_\phi = 27.38 \pm 0.07$ h and $P_\psi = 263 \pm 6$ h, respectively; the strongest observed lightcurve amplitude for the SAM case is in the 2nd harmonic of $P_1 = (P_\phi^{-1} - P_\psi^{-1})^{-1} = 30.56 \pm 0.01$ h. The rotation is retrograde with the angular momentum vector's ecliptic longitude and latitude of 250° and -75° (the uncertainty area is approximately an ellipse with the major and minor semiaxes of 27° and 14°, respectively). An implication of the retrograde rotation is a somewhat increased probability of the Apophis' impact in 2068, but it is still very small with the risk level on the Palermo Scale remaining well below zero. Apophis is a member of the population of slowly tumbling asteroids. Applying the theory of asteroid nutational damping by Breiter et al. (Mon. Not. R. Astron. Soc. 427, 755–769, 2012), we found that slowly tumbling asteroids predominate in the spin rate–size range where their estimated damping times are greater than about 0.2 Gyr. The appearance that the PA/NPA rotators transition line seems to follow a line of constant damping time may be because there are two or more asteroid spin evolution mechanisms in play, or the factor of μQ (the elastic modulus and the quality factor) is not constant but it may decrease with decreasing asteroid size, which would oppose the trend due to decreasing collisional age or excitation time.

Key words: Asteroid Apophis; Excited rotation; Photometry

1 Introduction

Aten-type asteroid (99942) Apophis was discovered by R.A. Tucker, D.J. Tholen and F. Bernardi at Kitt Peak, Arizona on June 19, 2004. After rediscovery by G.J. Garradd at Siding Springs, Australia in December 2004 it was recognized as a potentially hazardous asteroid with a significant Earth impact probability in April 2029. Arecibo radar observations in January 2005, August 2005 and May 2006 significantly reduced Apophis' orbital uncertainty and ruled out the 2029 impact (the minimum nominal distance from the geocenter in 2029 was computed to be 6 Earth radii), but other potential impacts in following decades were revealed. As the very close approach distance in 2029 turns a well determined pre-2029 orbit to a poorly estimated post-2029 orbit, even small perturbations prior to 2029 play a significant role. (See Farnocchia et al., 2013, for details and references on the progress in astrometric observations and orbit computations during 2004 to 2006.)

Chesley (2006), Giorgini et al. (2008) and Chesley et al. (2009) showed that the Yarkovsky effect (Bottke et al., 2006) significantly affects post-2029 predictions and they took it into account for Apophis impact predictions. Farnocchia et al. (2013) did a careful orbital analysis using selected best astrometric and radar data covering the interval 2004 March 15 to 2012 December 29 and quantified a sensitivity of predictions of the Earth impacts between 2060 and 2105 on physical parameters of the asteroid (diameter, albedo, density, thermal inertia, rotation period, and obliquity) that determine the rate of Yarkovsky drift of Apophis' semimajor axis. They estimated an impact probability greater than 10^{-6} for an impact in 2068. They also showed that further optical astrometric and radar observations will likely significantly constrain the Yarkovsky drift in late 2020 or 2021.

To put this formal detection in its true context, one must model the Yarkovsky accelerations as accurately as possible. A starting, and presently the most fundamental, step toward this analysis is to understand the rotation state of Apophis. This is because the sense of Apophis' rotation has been shown to be a critical element in predicting its possible future impacts. It would also allow to obtain an estimate of the asteroid's bulk density, which is a very important parameter as far as the potential impact hazard is concerned.

Raoul Behrend and his collaborators [1] took lightcurve observations during 2005 January 5 to February 1 and, assuming a principal axis (PA) rotation, estimated its spin period of 30.4 h. (Their formal error of 0.014 h is underestimated as they did not account for all uncertainty sources, and especially not for a possible systematic error due to the assumption of PA rotation.) The data blocks from different nights were on different (relative) magnitude scales and Behrend et al. applied offsets in their zero points for the fit; this approach would not allow them to reveal a potential non-principal axis rotation unless it had a high amplitude in other than the main period.

[1] http://obswww.unige.ch/~behrend/page_cou.html

Asteroids of sizes and spin rates similar to Apophis are often found to be in non-principal axis ("tumbling") rotation states. This is not surprising, considering their estimated damping times are comparable to or longer than the age of the solar system (Harris, 1994; Pravec et al., 2005). After excitation (e.g., by a sub-catastrophic collision; Henych and Pravec, 2013), their rotation would not be damped down to pure spin due to the energy dissipation from a stress-strain cycling within the tumbling body, as long as the rotation remains slow.

The spin state of Apophis can be described with the technique of lightcurve photometry. However, a huge amount of telescopic observing time is needed to get photometric data necessary to describe the spin state of a slow tumbling asteroid. To accomplish the task, it is needed to cover the long period multiple times (though the sampling rate may be relatively sparse). The large volume of photometric observations required could only realistically be obtained using small telescopes, thus requiring a favorable apparition with the asteroid bright enough and at sufficient elongation from the Sun. Apophis had such a favorable apparition from December 2012 to April 2013 when it could be observed with telescopes with sizes as small as 0.35 to 1.5 m. An additional requirement for description of tumbling was that the observations must be calibrated in a consistent magnitude system throughout the apparition. We collected such data through a collaborative campaign described in Section 2. Our analysis of the photometric data revealed that Apophis is indeed in a non-principal axis (NPA) rotation state (Section 3). We performed a physical modeling of the NPA rotation that we present in Section 4. In Section 5, we put Apophis in the context of the population of slowly tumbling asteroids.

2 Photometric observations

We took photometric observations of Apophis with the 1.54-m Danish telescope on La Silla (35 nights), the 0.41-m PROMPT 1 telescope on Cerro Tololo (30 nights), the 0.6-m TRAPPIST telescope on La Silla (4 nights), the 1-m telescope on Pic du Midi (3 nights), the 0.35-m telescope on Leura (3 nights), and the 0.65-m telescope in Ondřejov (1 night). Only good quality data that were calibrated in a consistent magnitude system were included in the dataset. The individual runs and their observational circumstances are listed in Table 1. The mid-time (UTC) of the run, rounded to the nearest tenths of day, is given in the first column. The asteroid's apparent right ascension and declination (equinox J2000.0) are given in the 2nd and 3rd column. In the next three columns, its geo- and heliocentric distances and solar phase angle are given. The telescope used is given in the last column.

The observations with the 1.54-m Danish telescope were taken with the Bessell R filter, with supplementary observations in the V filter on 2013 January 9, and they were calibrated in the Johnson-Cousins system using Landolt (1992) standard stars. Integration times were between 30 and 120 seconds and the

telescope was tracked at half-apparent rate of the asteroid, providing star and asteroid images of the same profile in one frame. For the Apophis' long period, we did not need to take continuous observations but we took a short series of typically five images once per hour or so, depending also on scheduling constraints of our other asteroid observations we ran on the nights; we worked Apophis as a secondary target on most of the 35 nights. We processed and reduced the data with our photometric reduction software package *Aphot32*.

The University of North Carolina at Chapel Hill's PROMPT observatory (Panchromatic Robotic Optical Monitoring and Polarimetry Telescopes) on Cerro Tololo consists of six 0.41-m telescopes outfitted with Alta U47+ cameras by Apogee, which make use of E2V CCDs. The field of view is $10' \times 10'$ with 0.59 arcsec/pixel. All raw image frames were processed (master dark, master flat, bad pixel correction) using the software package MIRA. Aperture photometry was then performed on the asteroid and three comparison stars. A master image frame was created to identify any faint stars in the path of the asteroid. Data from images with background contamination stars in the asteroid's path were then eliminated. The observations were done with Lum (IR block) filter and they were mutually linked in an instrumental magnitude system with an internal consistency of 0.02–0.03 mag.

The robotic 0.6-m telescope TRAPPIST (TRAnsiting Planets and PlanetesImals Small Telescope; Jehin et al. 2011) is located at ESO La Silla Observatory. Several image series with duration between 10 and 30 minutes were acquired each night. The camera is a FLI ProLine PL3041-BB with 2k×2k pixels of 15 μm. It was used with a special exoplanet filter (blue cut at 450 nm) and in the binning 2 mode, resulting in a pixel scale of 1.3 arcsec and a field of view of 22 arcmin. The telescope was tracking the asteroid. All the fields crossed by the asteroid were observed again on a photometric night in order to provide the best calibration. The obtained internal consistency is around 0.02 mag. The Exo magnitudes were converted to R band magnitude using TRAPPIST internal calibration system based on the regular observations of standard fields.

The observations with the 1-m telescope on Pic du Midi were performed with a sloan DSS, r' filter and a CCD 2V 2k×2k.

The observations with the 0.35-m telescope on Leura Observatory were taken and reduced using procedures described in Oey (2010). They were done in Clear filter and calibrated using solar colored comparison stars and Rc magnitudes derived from 2MASS catalog with internal consistency of 0.02-0.03 mag (Warner, 2007).

The Ondřejov 0.65-m observations were taken and reduced using procedures described in Pravec et al. (2006).

Each observatory's data were calibrated in its specific magnitude system. We converted them to the Cousins R system using data that mutually overlap with or were taken at times nearby to the observations from the 1.54-m Danish

telescope. While the 1.54-m data were calibrated in Cousins R with absolute errors of 0.01 mag, the absolute accuracy of the converted data from the other stations was somewhat lower and resulting absolute errors of the adjusted magnitude scale zero points of the individual sessions were estimated to be 0.02–0.03 mag.

Finally, to homogenize the data taken with different sampling rates, we averaged measurements taken from a single station on nearby times over a time span no longer than 0.3 h (1% of the Apophis' period), typically 5 consecutive data points were averaged; we suppressed averaging more than 7 measurements. The final dataset of Cousins R data consisting of 1098 observations (normal points) from 2012 December 23 to 2013 April 15 is available at http://www.asu.cas.cz/~ppravec/99942_lc_data.txt

3 Two-period analysis of the lightcurve data

Soon after the beginning of our observational campaign in December 2012, it became apparent that the brightness of Apophis did not repeat with a single period, but it showed a behavior characteristic for tumbling asteroid. We analysed the data using the 2-period Fourier series method (Pravec et al., 2005). A basic assumption of the method is that changes of the asteroid lightcurve due to evolution of the asteroid-Earth-Sun geometry during the analysed data time span are negligible. As the Apophis' solar phase as well as its geo- and heliocentric position vectors changed substantially during the full observed apparition December 2012 to April 2013, we limited our period analyses to the best covered interval 2013 January 7 to February 19. In this interval the solar phase was between 32.4° and 52.9°; we did not include the less abundant data taken in the first two and the last five weeks of the apparition when the solar phase was higher (between 54° and 78°). We did the fits and period analyses with the photometric data reduced to the unit geo- and heliocentric distances and to a consistent solar phase using the H–G phase relation, assuming the mean $G = 0.24$ for S type [2] asteroids (Warner et al., 2009), and converted to flux units (luminosities). We used the 3rd order 2-period Fourier series; a use of higher orders, though they might be needed to describe some smaller features of the lightcurve, was not justified with the available data as it would give poorly determined fits as we checked.

We found that in all meaningful fits, the highest signal was always in the second harmonic of a period of 30.56 h (formal uncertainty < 0.01 h). Amplitudes in all other harmonics of the two fitted frequencies or their linear combinations were smaller by a factor greater than 2. The lightcurve of Apophis re-

[2] Apophis was found to be an Sq-class asteroid by Binzel et al. (2009). Our measured $(V-R) = 0.453 \pm 0.01$ is consistent with the classification. We also derived the mean absolute magnitude of Apophis of $H = 19.09 \pm 0.19$, assuming $G = 0.24 \pm 0.11$ that is the slope parameter range for S and Q types (Warner et al., 2009).

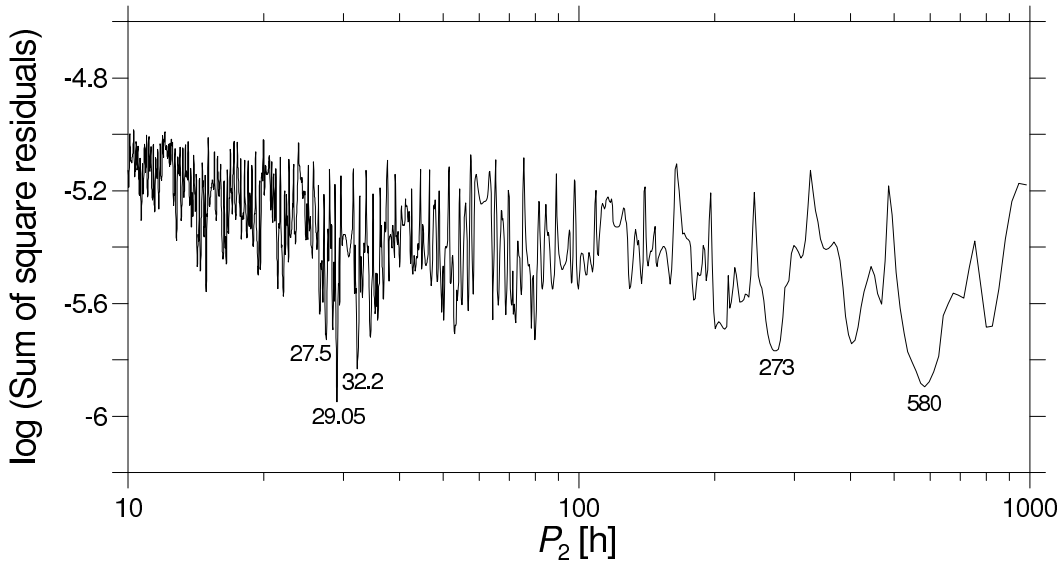

Fig. 1. The sum of square residuals vs P_2 for the 3rd order 2-period Fourier series with $P_1 = 30.56$ h fitted to the Apophis' reduced data in flux units (arbitrary scale) taken from 2013 January 7 to February 19. Five periods providing best fits are marked, but some of them are related (see the text).

sembled simulated lightcurves of tumblers in Short-Axis Mode with the mean wobbling angle 20–25° (Henych and Pravec, 2013); we preliminarily concluded that Apophis' rotation is only moderately excited. In our further analyses, we assumed that this most prominent period $P_1 = 30.56$ h is $P_1^{-1} = P_\phi^{-1} - P_\psi^{-1}$, where P_ψ is a period of rotation of the body around its shortest principal axis and P_ϕ is the time-averaged period of precession of this axis around the angular momentum vector (Kaasalainen, 2001). This assumption was confirmed in our later physical modeling (see Section 4).

In Fig. 1, we plot a sum of square residuals vs P_2 for the fitted 3rd order 2-period Fourier series with $P_1 = 30.56$ h and P_2 sampled using a grid with variable step to ensure a sufficiently dense sampling of the period. We found a few P_2 values that give a satisfactory fit to the data. The best fit was obtained with a period of 29.05 h, but there were other nearby periods that gave only slightly poorer fits; we marked there the periods 32.2 h and 27.5 h in the plot. The long periods of ~ 273 and ~ 580 h are tied to the 27.5 and 29.05 h periods, respectively; note that $27.5^{-1} - 30.56^{-1} \doteq 273^{-1}$ and $29.05^{-1} - 30.56^{-1} \doteq 580^{-1}$. In Fig. 2, we present a composite lightcurve of the reduced photometric data and the fitted 3rd order 2-period Fourier series for the periods $P_1 = 30.56$ h and $P_2 = 29.05$ h.

An interpretation of the obtained candidate P_2 periods is not unique. Pravec et al. (2005) and Scheirich et al. (2010) found that for the two Long-Axis Mode (LAM) tumblers 2002 TD60 and 2008 TC3, their P_2 values correspond to P_ψ and P_ϕ, respectively. Analysing the photometric data from Spencer et al. (1995) taken at solar phases $< 42°$ for the best described tumbling asteroid (4179) Toutatis (again a LAM case), Pravec et al. (2005) obtained P_2 equal to $P_\psi = 130$ h found by Hudson and Ostro (1995). P_1 values of

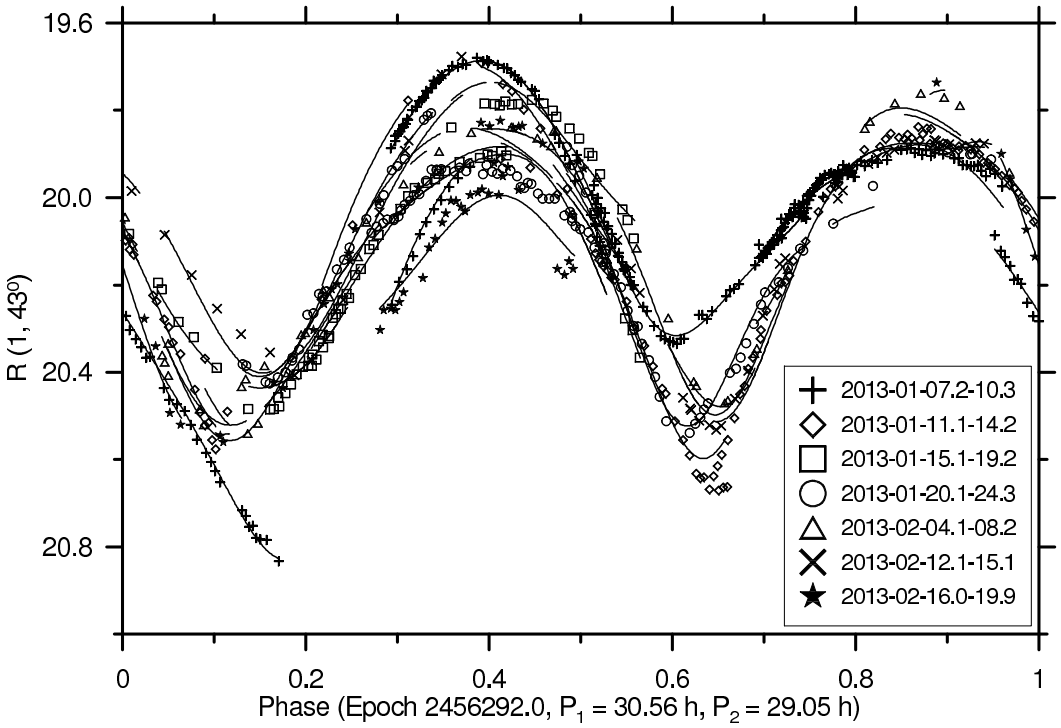

Fig. 2. Apophis' Cousins R measurements reduced to the unit geo- and heliocentric distances and to solar phase 43°, assuming the phase relation's slope parameter $G = 0.24$, are plotted folded with the period P_1. The curves are sections of the best fit 3rd order Fourier series with the periods 30.56 and 29.05 h.

the three LAM tumblers are either the other of the two periods $\{P_\psi, P_\phi\}$, or $(P_\phi^{-1} + P_\psi^{-1})^{-1}$. From these three cases, we tentatively (being aware of that it is only a statistics of three) suggest that for highly excited tumblers in Long Axis Mode and with photometric data taken at non-extreme phase angles and over a limited range of geo- and heliocentric asteroid positions, periods found using the 2-period Fourier series method correspond to two of the three periods $\{P_\psi, P_\phi, (P_\phi^{-1} + P_\psi^{-1})^{-1}\}$.

In the case of Apophis, however, we must be more careful. In contrast with the cases of Toutatis, 2002 TD60 and 2008 TC3 where the amplitudes in the harmonics of P_2 were almost as high (well within the factor of 2) as in P_1, the amplitudes in the harmonics of all the candidate P_2 for Apophis were substantially smaller than the amplitude of the second harmonic of $P_1 =$ 30.56 h. This moderate P_2 amplitude might cause the 2-period analysis of the Apophis data to be more sensitive to lightcurve shape changing effects, which might be also stronger because the observations of Apophis were taken at higher solar phases and over a wider range of geo- and heliocentric positions than the above LAM cases. In particular, there could be present an amplitude-phase effect (Zappalà et al., 1990), and changes of the viewing aspect (the angle between the asteroid-Earth vector and the asteroid's angular momentum vector) could have a significant effect too. So, unlike in the similar analysis of photometric observations of 2008 TC3 in Scheirich et al. (2010), we were not sure whether we could take some of the periods $P_2 = 29.05$, 32.2 and 27.5 h

suggested from the 2-period analysis as candidates for P_ψ or P_ϕ, but rather we searched for the rotation and precession periods of the NPA rotation of Apophis using a physical model as described in the next section.

4 Physical model

A method of construction of physical models of tumbling asteroids was developed and described by Kaasalainen (2001). We perform an optimization of the dynamical parameters of the body including derivation of its shape using a code developed by M. Kaasalainen that we used for modeling of 2008 TC3 (Scheirich et al., 2010) and further developed since then. The main points of the inversion method are following.

The asteroid NPA rotation is described with the following eight parameters:

- I_a and I_b are the moments of inertia for the longest (for Short Axis Mode) or shortest (for Long Axis Mode) and the intermediate principal axes of the body's ellipsoid of inertia, respectively. The principal moment I_c is normalized to unity. We use the notation where c is always the axis around which the body is seen as rotating.

- λ_L and β_L are the ecliptic coordinates of the angular momentum vector $\vec{L}$. It is constant in absence of external forces, and the c axis precesses around it.

- ϕ_0 and ψ_0 are the Euler angles describing the orientation of the asteroid at epoch t_0. We use the angles in the so-called x-convention (see Samarasinha and A'Hearn, 1991). The Z axis of the inertial frame is parallel to $\vec{L}$ and the XZ plane contains a vector pointing to the vernal equinox. The third Euler angle, θ, is directly related to the other parameters (see Kaasalainen, 2001) and therefore it is not used as an independent parameter. Time evolution of the whole set of Euler angles, permitting transformation from the body-fixed frame to an inertial frame of choice, is obtained by numerical integrations of Euler equations. As there occur various conventions of describing asteroid orientation in literature, we explicitly describe the convention we use in Appendix A to avoid confusion.

- P_ψ and P_ϕ are the period of rotation around the c axis and the time-averaged period of precession of the axis around $\vec{L}$, respectively.

Since the lightcurve of Apophis only moderately deviates from a principal axis rotator lightcurve, our working hypothesis was that the asteroid is in SAM with a low level of excitation. Since the evolutions of the Euler angles ϕ and ψ have the opposite directions for SAM, we assumed that the main lightcurve frequency P_1^{-1} is the difference of the precession and rotation frequencies. We therefore tested combinations of P_ϕ and P_ψ satisfying $P_\phi^{-1} - P_\psi^{-1} = P_1^{-1} = 1/30.56$ h.

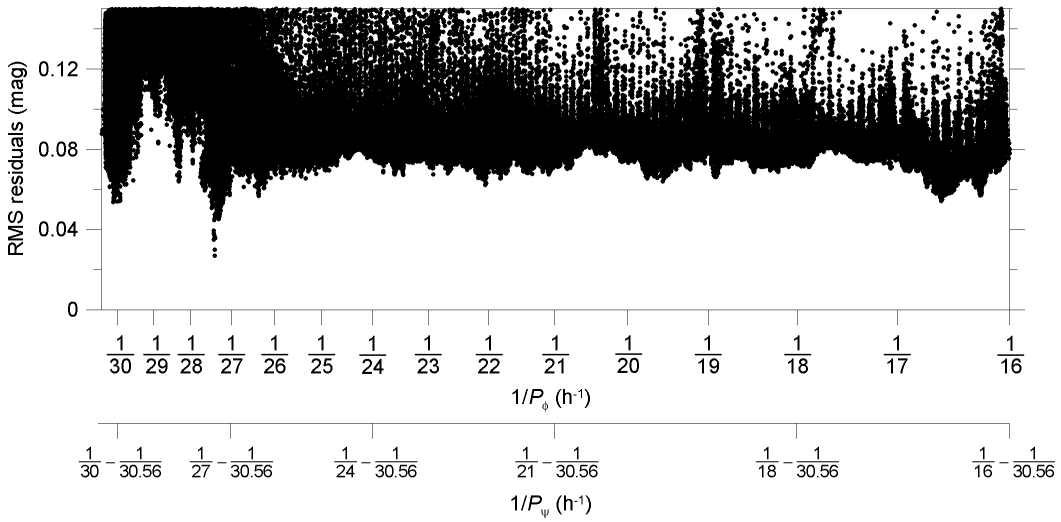

Fig. 3. The root mean of square residuals vs the periods P_ϕ and P_ψ. Each point represents a result of the optimization starting from one point of the initial grid (see text). The best-fit solution has the RMS residual of 0.027 mag.

P_ϕ was searched from 16.0 to 30.3 h with a step of 0.1 h, with P_ψ computed from the above relation. At each step, we constructed a grid of (λ_L, β_L, ϕ_0, ψ_0). Using the periods and the parameter values from the grid as initial guesses, an optimization of convex shape and all eight parameters was performed. An initial shape for optimization was set to be a slightly elongated ellipsoid with semiaxes $a/c = 1.10$ and $b/c = 1.05$ (a sphere would lead to degeneracy in parameters describing the shape and in an invalid first step of iteration). In order to increase the optimization speed as well as to construct a plot of the root-mean-square (RMS) residuals of the fit vs the periods, we adapted the code so that P_ϕ did not diverge by more than 0.06 h from the initial value during the optimization. The plot of the RMS residuals vs the periods is shown in Fig. 3.

The photometric behavior of the surface was described by Hapke's photometric function for a rough surface (Hapke, 1993) with parameters $w = 0.369$, $g = -0.308$, $h = 0.11$, $S_0 = 0.16$, $\bar{\theta} = 20°$, which are typical for an S type asteroid. We found that the model is only weakly sensitive to these parameters.

We found a unique model solution. The angular momentum vector's orientation is retrograde. The parameters of a nominal solution that lies in the center of the uncertainty area of λ_L and β_L shown in Fig. 4 and their admissible errors that correspond to 3σ confidence level (see Scheirich and Pravec, 2009) are given in Table 2. (This nominal solution is close to the formal best fit solution, their difference is insignificant.) We report two kinds of axial ratios. $a_{\rm dyn}/c_{\rm dyn}$ and $b_{\rm dyn}/c_{\rm dyn}$ are axial ratios of a dynamically equivalent ellipsoid, i.e., a homogeneous ellipsoid with the same values of principal moments of

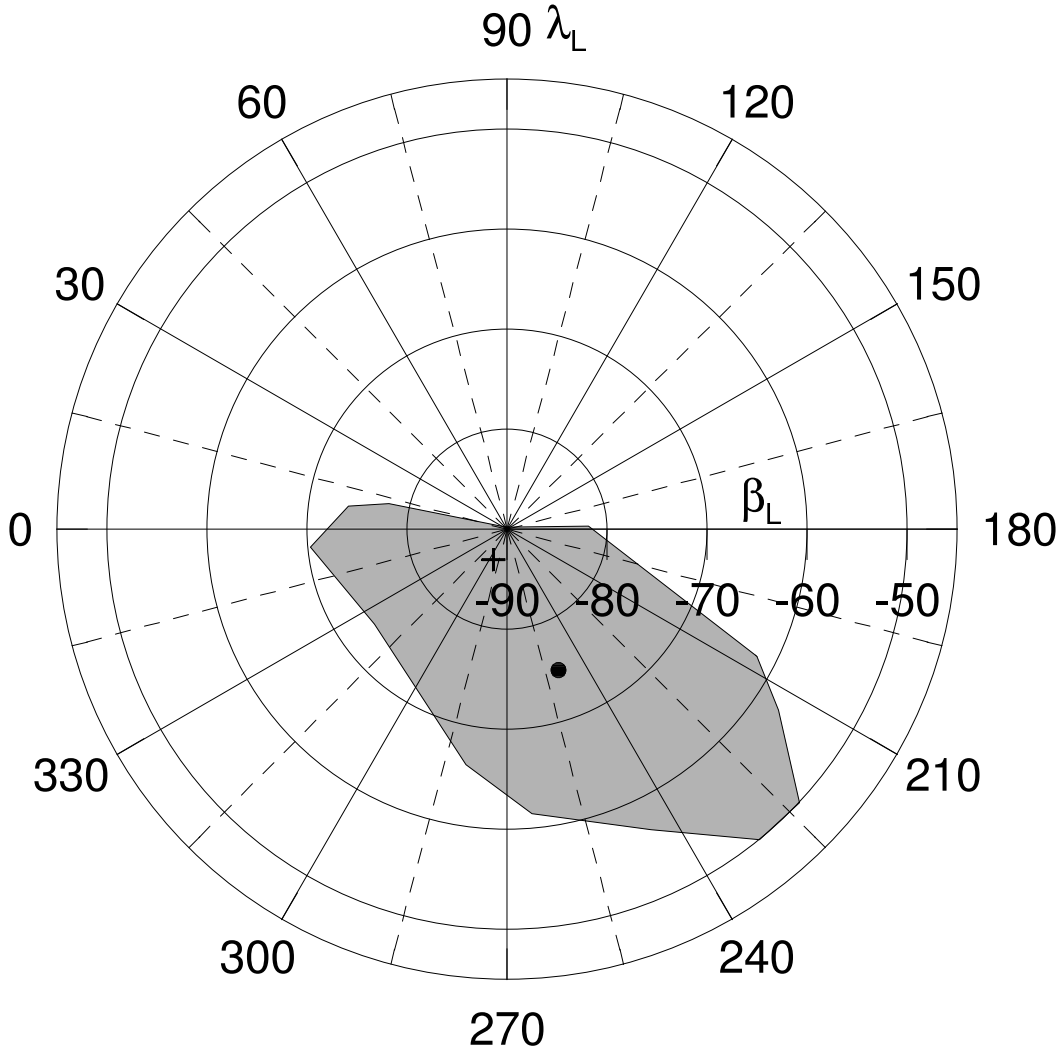

Fig. 4. Area of admissible directions of the angular momentum vector in ecliptic coordinates (grey area). The dot is the nominal solution given in Table 2. This area corresponds to 3σ confidence level. The south pole of the current asteroid's heliocentric orbit is marked with the cross.

inertia I_a and I_b, they are defined as:

$$\left(\frac{a_{\rm dyn}}{c_{\rm dyn}}\right)^2 = \frac{I_b - I_a + 1}{I_a + I_b - 1}, \quad \left(\frac{b_{\rm dyn}}{c_{\rm dyn}}\right)^2 = \frac{I_a - I_b + 1}{I_a + I_b - 1}. \tag{1}$$

$a_{\rm shp}/c_{\rm shp}$ and $b_{\rm shp}/c_{\rm shp}$ are axial ratios of an ellipsoid with the same values of principal moments of inertia as the fitted convex shape, both assumed homogeneous. Moments of inertia of the best fit convex shape are lower than the best-fit values of I_a and I_b by 5% and 4%, respectively, but their 3σ error bars mutually overlap.

The angles θ_{min}, θ_{max} and θ_{aver} presented in Table 2 are minimum, maximum, and time-averaged values of the wobbling angle.

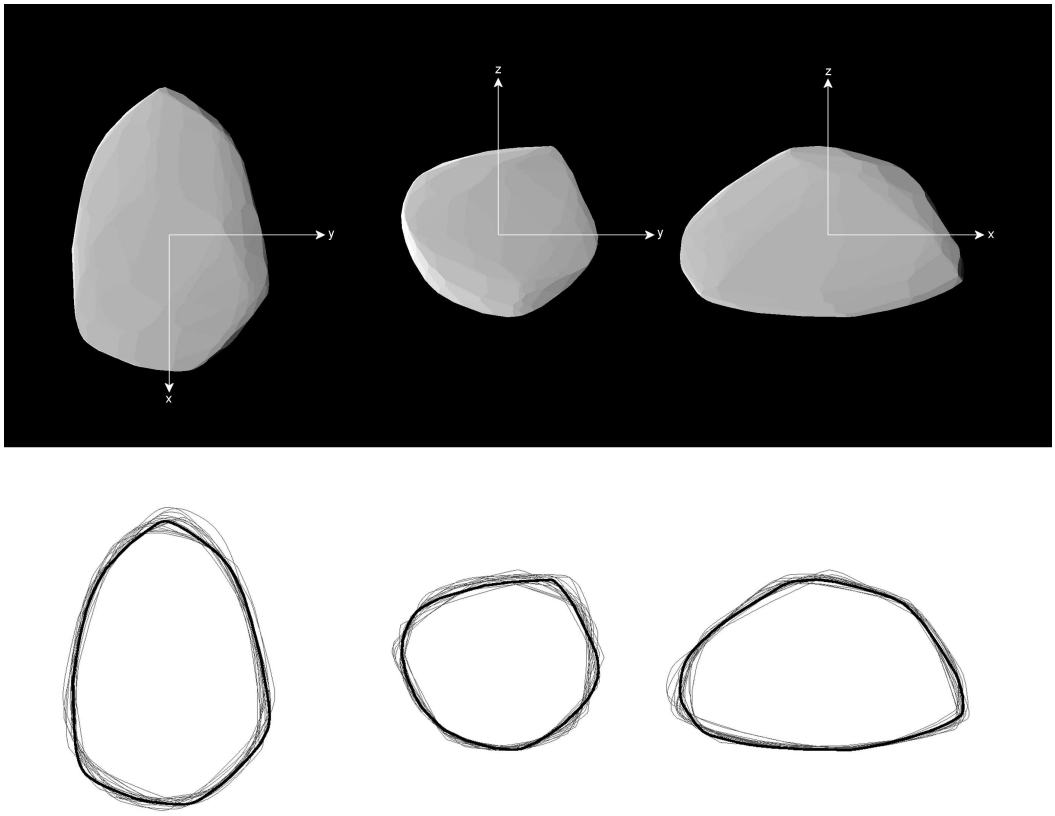

Fig. 5. Top: The convex shape model of the nominal solution given in Table 2 shown in three viewing geometries; x and z are the principal axes with the smallest and greatest moments of inertia, respectively. Bottom: Silhouettes of the nominal convex shape model (bold curve) and for a sample of solutions covering the admissible uncertainty solution range (thin curves).

The convex shape model of the nominal solution is presented in Fig. 5, top panel. From the shape models of solutions lying in the admissible uncertainty area, we show silhouettes of those that differ to the most extreme in different directions from the nominal solution shape in the bottom panel of the figure. All the silhouettes are plotted for the shapes normalized to the same volume of the dynamically equivalent ellipsoid (i.e., $a_{\rm dyn}b_{\rm dyn}c_{\rm dyn} = {\rm const.}$) and with the principal axes in the same orientation as in the top panel. The synthetic lightcurve of the best fit model together with the observational data is presented in Fig. 6.

We also checked a possibility that $P_2 = 29.05$ h (see Section 3) is one of the periods P_ϕ or P_ψ, or that the rotation and precession periods are a linear combination of P_1 and this P_2. LAM and SAM modes were tested for each of these combinations (18 in total) using the shape fitted as triaxial ellipsoid. None of these tests gave a satisfactory fit to the observational data.

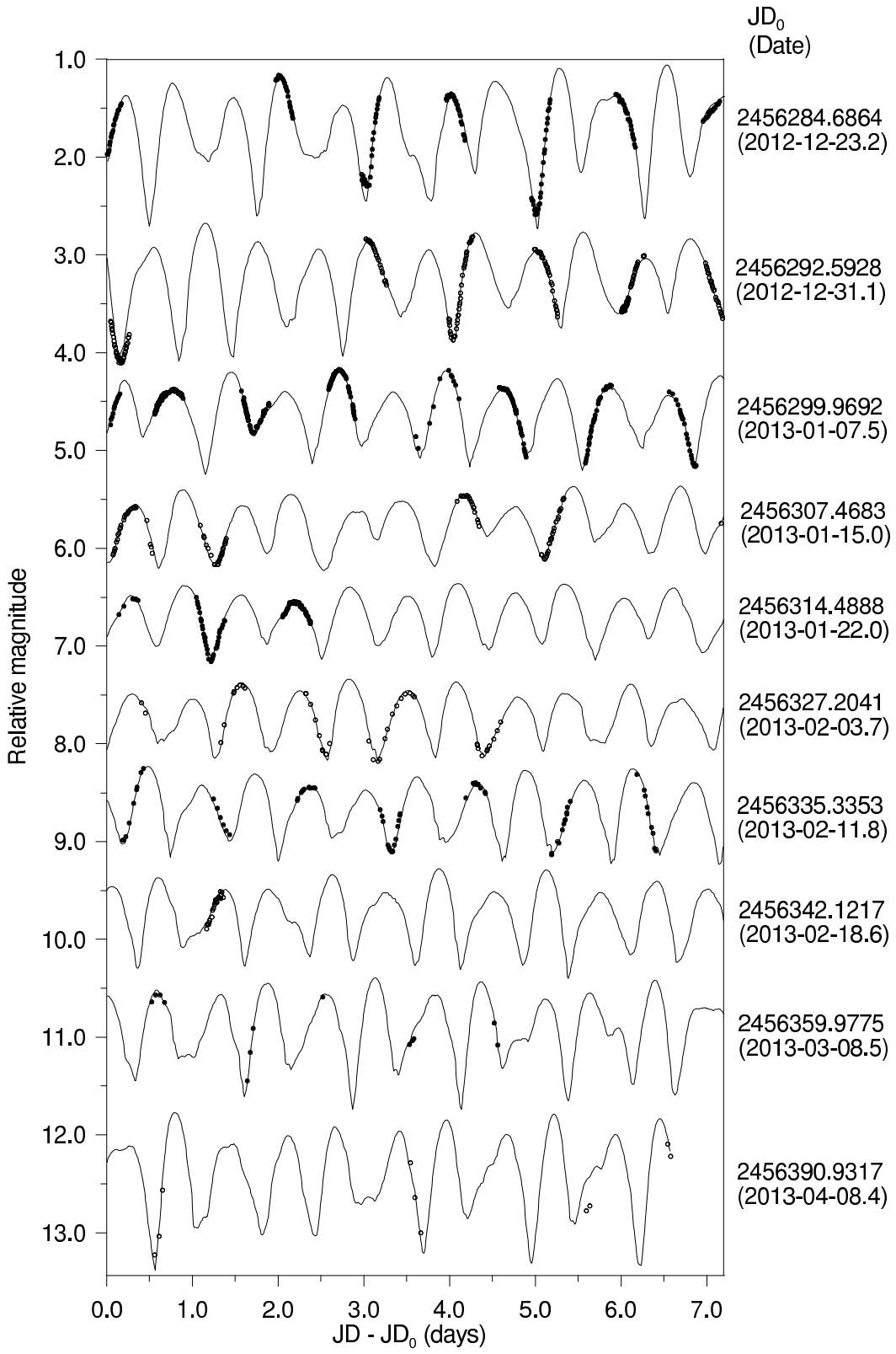

Fig. 6. The lightcurve data points and the synthetic lightcurve for the best fit solution (solid line). The magnitude scales of individual blocks were offset for clarity.

The shape and rotational state of Apophis are interesting in two points: (1) The greatest and intermediate moments of inertia differ by 3–4% only. (2) The asteroid is relatively close (energetically) to the basic rotation state, the rotational kinetic energy E is greater than the minimum kinetic energy E_0 (for rotation around the principal axis with the greatest moment of inertia) by only 2–3%. Despite this low-energy level of excitation, the figure dynamically close to a prolate ellipsoid causes that the wobbling angle reaches substantial values with $\theta_{\max}$ of 50–60°. If the shape was more different from a prolate ellipsoid with I_b substantially lower than 1, the asteroid would show a lower tumbling amplitude. For instance, if it was dynamically equivalent to an oblate ellipsoid with $I_b = I_a = 0.61$, we would get a precession angle [3] of $\theta' = 18°$. The exaggeration of the tumbling amplitude in near prolate ellipsoid asteroids with small difference between I_2 and I_3 can facilitate detection of the tumbling even for a low excitation level. On the other hand, the nearly prolate ellipsoid shape could suppress amplitudes in the harmonics of the second lightcurve frequency and their combinations with the main frequency, hence limiting detectability of the tumbling. Yet the real shape may differ from a prolate ellipsoid more than its dynamically equivalent ellipsoid, thus increasing the lightcurve amplitudes again. For combination of the opposing effects, a future work should reveal what is the average net effect of a near prolate ellipsoid shape on the detectability of tumbling and whether I_b close to 1 rather facilitates or hampers detection of asteroid tumbling.

A question arises whether Apophis is so close (energetically) to the basic rotation state just by chance (in a case the excitation energy distribution is about uniform), or whether the fact that it experienced a relatively low-energy excitation event is rather a norm; for some spin excitation mechanisms, lower energy excitation events would be more frequent, e.g., for smaller impactors being more frequent (see the next section for possible asteroid rotation excitation mechanisms). A possibility that the Apophis' tumbling could be substantially damped from a higher level set by an early excitation event that happened a long time ago is unlikely, given its long damping time (see Section 5.1). Further studies of tumbling asteroids should show whether Apophis is an outlier or a typical member of the slow tumbling asteroid population.

4.1 Implications for impact predictions

There are interesting implications of the retrograde rotation of Apophis for its impact predictions. Farnocchia et al. (2013) analysed future orbital evolution of Apophis and determined a detailed distribution of the post-2029 impacts

[3] The minimum and maximum values for the precession angle θ' (see Black et al., 2009) are

$$\tan\theta'_{\min,\max} \equiv \frac{\omega_{1,2}}{\omega_3} = \left[\frac{\frac{E}{E_0} - 1}{I_{a,b}(1 - \frac{E}{E_0} I_{a,b})}\right]^{\frac{1}{2}}. \quad (2)$$

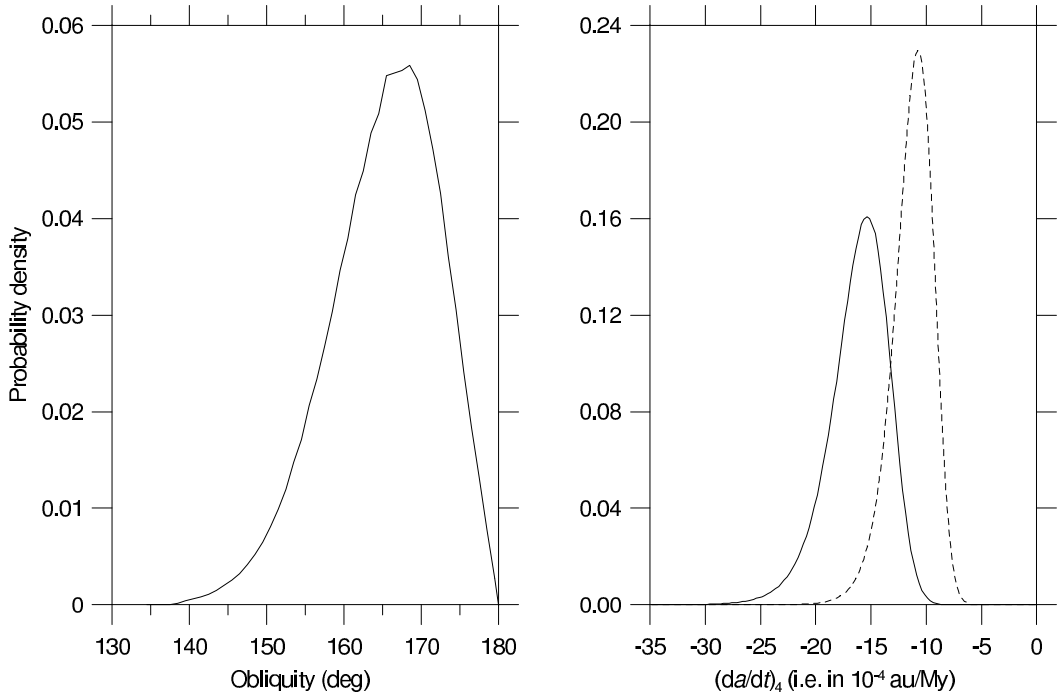

Fig. 7. Left panel: Probability density for the tilt between Apophis' angular momentum vector $\vec{L}$ and the normal to its heliocentric orbit (used as a proxy for the obliquity here). Right panel: Probability density of the estimated secular drift of the Apophis' semimajor axis (in 10^{-4} au/My units). The effects of non-sphericity and weak NPA rotation state would decrease the da/dt values by a factor of about 0.6–0.8; the dashed curve exemplifies the effect of scaling by a factor of 0.7.

keyholes in the 2029 encounter b-plane. By taking into account the effects of thermal accelerations they noted that a number of the keyholes were located in the uncertainty region of the 2029 orbit prediction. Folding this information together they finally derived probabilities for several future impact events. The thermal accelerations depend on a number of parameters, including the asteroid's size and surface thermal inertia, however the main uncertainty was the unknown rotation state. Farnocchia et al. (2013) thus circumvent the situation by considering a generic obliquity distribution of near-Earth asteroids, allowing for both prograde and retrograde rotation sense. Our results now fundamentally collapse this main uncertainty to a much narrower zone.

In the following simple test we shall use the tilt between Apophis' rotational angular momentum vector $\vec{L}$ and the normal to its heliocentric orbit as a proxy of the spin obliquity. Figure 7 (left panel) shows the probability density for the obliquity from our solution. The median obliquity is 165° and the 1σ-like range (from the 16th to the 84th percentile) is 157 to 172°. With it, we repeated the analysis of Farnocchia et al. (2013) and obtained an estimate of the secular drift of Apophis' heliocentric semimajor axis using a simplified linear heat diffusion theory for a spherical body (e.g., Vokrouhlický, 1999). The effects of non-sphericity should result in a decrease of the estimated da/dt values by a factor of about 0.8–0.9 (e.g., Vokrouhlický, 1998). The effect of NPA rotation

state would, in the zeroth approximation, be accounted for by taking the spin axis along the rotation angular momentum vector $\vec{L}$ and a shape corresponding to a convex hull swept by Apophis during many precession cycles in ψ and ϕ Euler angles (note that taking the spin along $\vec{L}$ produces reasonable results even for the extreme tumbling case of (4179) Toutatis; e.g., Vokrouhlický et al., 2005). This would result in a decrease of the estimated $\mathrm{d}a/\mathrm{d}t$ values by another factor of $\sim 0.8 - 0.9$ (e.g., Vokrouhlický, 1998). Overall, the semimajor axis drift based on the simplified theory of spherical bodies would overestimate the expected value by a factor of $\sim 0.6 - 0.8$ (Fig. 7, right panel).

The take-away message follows from comparison of our estimated $\mathrm{d}a/\mathrm{d}t$ values in Fig. 7 and those of Farnocchia et al. (2013, their Fig. 3). We note the huge decrease of the range of estimated $\mathrm{d}a/\mathrm{d}t$ values which directly reflects in a decrease of uncertainty in the principal direction of Apophis' location in the b-plane of the 2029 encounter (Farnocchia et al., 2013, Fig. 6). We predict that our spin solution for Apophis virtually removes any possibility of the 2069 impact as its keyhole requires $\mathrm{d}a/\mathrm{d}t$ values outside our constrained range, but interestingly increases the probability of the impact on 2068 April 12.6. Farnocchia et al. (2013) estimated the probability of impact of Apophis on that date to be 2.3×10^{-6}. Our estimated range of $\mathrm{d}a/\mathrm{d}t$ values contains the range they computed as required for the 2068 impact keyhole, i.e., resulting in an increased probability of the impact. Anyway, the risk level on the Palermo Scale remains well below zero, and it remains zero on the Torino Scale. A detailed determination of the thermal accelerations in Apophis' orbit, taking also into consideration its tumbling state (along the lines of analysis in Vokrouhlický et al., 2005), and a new determination of future impact probabilities for Apophis will be done in a forthcoming study.

5 Population of tumbling asteroids

Apophis is a member of the population of slowly rotating tumbling asteroids. Tumblers predominate at spin rates where the time of damping of excited asteroid rotation by internal energy dissipation is comparable to or longer than the time scale of rotation excitation, or at most the age of the solar system (Harris, 1994; Pravec et al., 2005).

We took the opportunity of finding Apophis in a tumbling state to get an up-to-date picture of the slow tumblers population. To that goal we checked lightcurve data for all asteroids from the Asteroid Lightcurve Database (LCDB, version 2013 September; Warner et al. 2009) with estimated diameters between 0.2 and 100 km and the damping time $T_\mathrm{d} > 0.0045$ Gy calculated with eq. (11) below. This limit corresponds to the damping timescale $\tau \gtrsim 0.045$ Gy estimated with the earlier formula of Harris (1994), see also eq. (5) in Pravec et al. (2005). [4] The reason for the choice of the lower diameter limit of 0.2 km

[4] We designate the damping timescale estimated with the Harris (1994) formula

is that it is the lower limit of the size range where asteroids of cohesionless structure held together by self-gravitation only predominate (Pravec et al., 2007); smaller asteroids are mostly superfast rotators and they may have a different internal structure, and we plan to study their NPA rotations in a separate paper. The upper size limit of 100 km was chosen because the largest known slow rotators are about 80–90 km in diameter, and the largest known tumbling asteroid is (253) Mathilde with estimated diameter about 58 km (Mottola et al., 1995). For each asteroid in the given size and $T_{\rm d}$ range, we checked their lightcurve data and assigned them a PAR code as defined in Pravec et al. (2005). A value of PAR $\geq +2$ means that the given asteroid is in a state of principal axis rotation or close to it; a low-magnitude tumbling with the mean wobbling angle less than $\sim 15^\circ$ is not recognizable with ordinary lightcurve observations (Henych and Pravec, 2013). A value of PAR ≤ -2 indicates that the asteroid was recognized to be a tumbler. We provide a file with the PAR codes assigned to individual asteroids available at http://www.asu.cas.cz/~ppravec/pardat_20130917.txt

In Fig. 8, we highlighted asteroids in the studied size and $T_{\rm d}$ range with PAR ≤ -2 (red diamonds) and PAR $\geq +2$ (green squares). Note that for most asteroids in the LCDB in the given diameter–damping time range, we were not able to constrain their PA or NPA rotations (they obtained $|{\rm PAR}| \leq 1$). This is because observations of slowly rotating tumblers are very demanding; it requires a huge amount of observations covering the long period repeatedly, and the data must be calibrated in a consistent magnitude system. Such data are typically taken for only a fraction of observed long period asteroids, hence only a small sample of them could be uniquely recognized as being in PA or NPA rotation state and get $|{\rm PAR}| \geq 2$. The observed distribution of PA/NPA rotators constrains a few things that we will discuss in Sect. 5.2.

A fundamental question is what rotation excitation and damping mechanisms work in asteroids. The following excitation mechanisms were proposed: (1) original tumbling resulted from the formation of asteroid in disruption of its parent body, (2) sub-catastropic impacts (Henych and Pravec, 2013, and references therein), (3) spin down by the YORP effect (Vokrouhlický et al., 2007; Breiter et al., 2011), (4) gravitational torques during planetary flyby (Scheeres et al., 2000, 2005). A proposed mechanism for damping of excited rotation is the energy dissipation due to a stress-strain cycling within tumbling body (Burns and Safronov, 1973; Harris, 1994; Efroimsky, 2001; Sharma et al., 2005; Breiter et al., 2012).

Before looking at what the data for tumbling and non-tumbling asteroids reveal and how they constrain the rotation excitation/damping theories, we are going to look at how to best estimate damping times for our observed asteroids in PA and NPA rotation states. We aim to replace the old Harris (1994) formula for estimating the damping time with one derived using more recent nutational damping theories. While adopting the approach of Breiter et

as τ, to distinguish it from the damping times $T_{\rm d}$ estimated with the new theories described in Section 5.1.

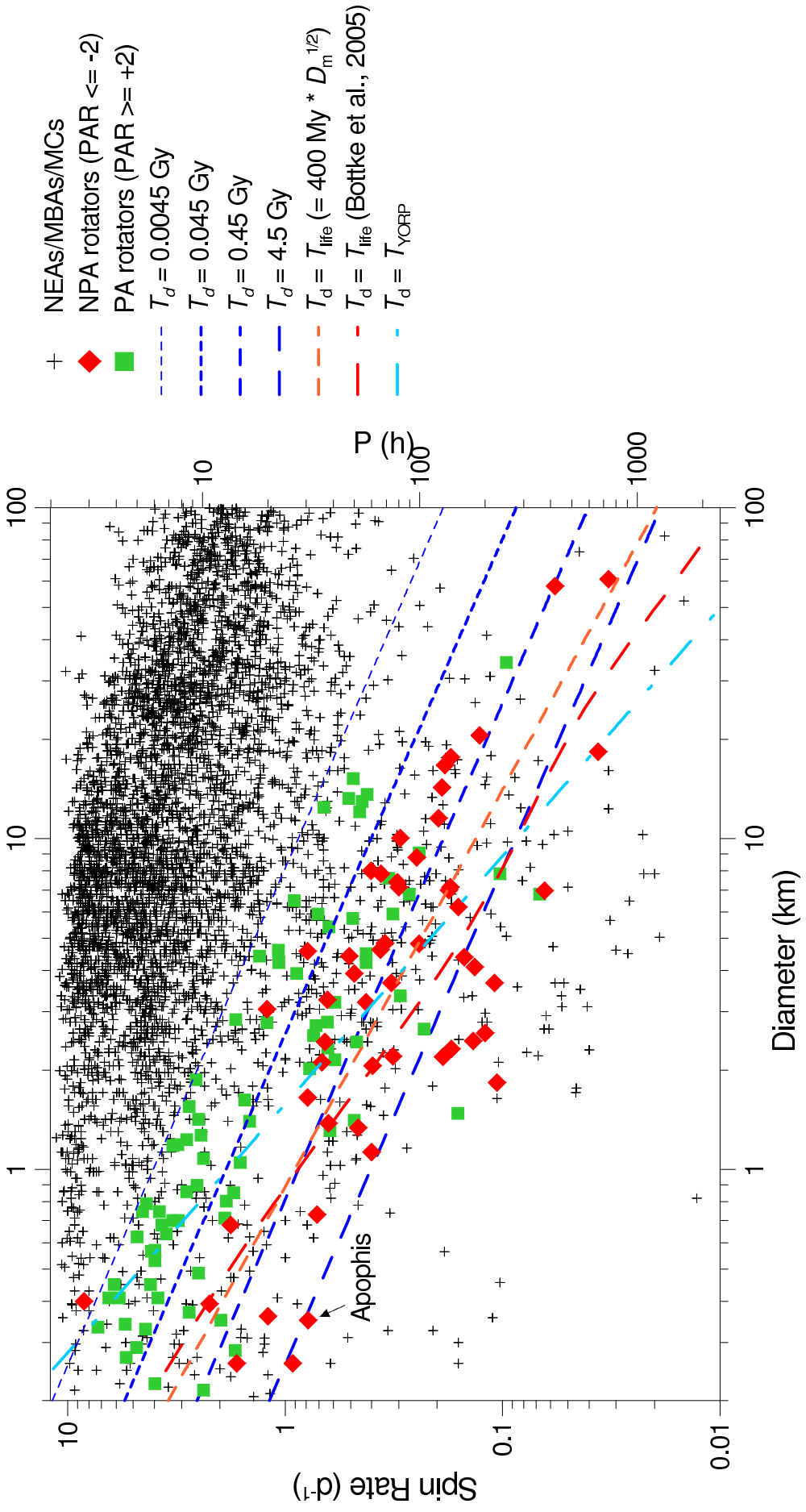

Fig. 8. Spin rate vs diameter data for asteroids from the LCDB (version 2013 September) with period quality code $U \geq 2$. Among asteroids with estimated $T_{\rm d} > 0.0045$ Gy, recognized tumblers (PAR ≤ -2) are marked with red diamonds and apparent PA rotators with green squares. See Section 5.2 for description of the plotted lines and curves.

al. (2012) as the state-of-art model below, we also complement their results by those from a model by Sharma et al. (2005) for completeness. This is because both models took a little different angle of view for how to define reference energy to be dissipated by internal anelastic processes and one might wonder, how this affects final results to be used in comparison with observations. We show that, in spite of earlier claims, our definitions of reference parameters make their differences relatively small.

5.1 Asteroid nutational damping time

5.1.1 Breiter et al. (2012) theory

Breiter et al. (2012) found that the nutational damping time for a self-gravitating, triaxial ellipsoid with the semiaxes $a \geq b \geq c$ is

$$T_{\mathrm{d}} = D(h_1, h_2)\frac{\mu Q}{\rho a^2 \tilde{\omega}^3}, \tag{3}$$

where $D(h_1, h_2)$ is a shape parameter defined below, μ is the elastic modulus, Q is the quality factor, ρ is the density, a is the semi-major axis of the ellipsoid, $\tilde{\omega}$ is an angular velocity of the ellipsoid with the same angular momentum damped to the basic state of rotation around the principal axis with the maximum moment of inertia, i.e.,

$$\tilde{\omega} = \frac{L}{I_3}, \tag{4}$$

where L is the ellipsoid's angular momentum and I_3 is the moment of inertia around its shortest principal axis. The shape parameter is

$$D(h_1, h_2) = -\frac{h_1^2(1+h_1^2)(1-h_2^2)}{5(1+h_1^2 h_2^2)} \int_{\theta_{\mathrm{i}}}^{\theta_{\mathrm{f}}} \frac{\sin\theta\cos\theta}{\Psi_3}\mathrm{d}\theta, \tag{5}$$

where θ_{i} and θ_{f} are the initial and the final maximum wobbling angle, respectively, $h_1 \equiv b/a$, $h_2 \equiv c/b$, and Ψ_3 is a dimensionless factor of the energy loss rate (Breiter et al., 2012). Above, we omitted the subscript '3' that Breiter et al. used for some of the quantities to mark that the formula is valid for damping in Short Axis Mode (SAM). As the damping in Long Axis Mode (LAM) is much faster, we take the SAM damping time as a satisfactory approximation for the total damping time even for an initial state of LAM. In their Fig. 1, Breiter et al. plot the calculated damping times for a family of ellipsoids with $h_1 = h_2 = h$, $\theta_{\mathrm{i}} = 85°$, $\theta_{\mathrm{f}} = 5°$, and assuming $a = 1\,\mathrm{km}$, $\rho = 2000\,\mathrm{kg\,m^{-3}}$, $\mu = 10^9\,\mathrm{Pa}$ and $Q = 100$. In their Fig. 2, they plot $D(h)$ for the same parameter values except for $\theta_{\mathrm{i}} = 45°$.

For application to the observational data for tumbling asteroids, we need to adapt the Breiter et al.'s damping time calculation in following points.

(1) In eq. (3), we substitute $a \equiv D_{\rm m}/(2h)$, where $D_{\rm m}$ is the asteroid mean diameter, i.e., the diameter of a sphere with the same volume. The reason is that for ellipsoids with $h_1 = h_2 = h$ observed at random aspects, observations provide straightforward estimates of the mean diameter [5] rather than a. The adapted eq. (3) is

$$T_{\rm d} = D(h,h)\frac{4h^2\mu Q}{\rho D_{\rm m}^2 \tilde{\omega}^3}. \tag{6}$$

(2) We assume $h = 0.7$ as default. The reason is that observed tumbling asteroids appear to have about typical asteroid elongations on average.

(3) We use $D(h) = 20.4$ for $h = 0.7$ that S. Breiter (personal communication) calculated for damping from $\theta_{\rm i} = 85°$ to $\theta_{\rm f} = 15°$. The reason for the choice of the lower limit of 15° is that with standard photometric observations, the minimum detectable mean wobbling angle is 10–15° (Henych and Pravec, 2013), hence we take the lower limit on the maximum wobbling angle of 15°. The value of $D(h)$ is rather sensitive to the actual lower limit on θ as the damping is slow at low wobbling angles; S. Breiter calculated $D(h) = 39.2$ for $h = 0.7$ and damping to 5°, which is greater by a factor of 1.92 than the adopted value for damping to 15°. The choice of the upper limit is less critical as the damping is fast at high wobbling angles; a value of $D(h)$ for $h = 0.7$ and damping from 45° to 15° is 15.5, i.e., less by only a factor of 1.32 than the adopted value for damping from 85°.

(4) In eq. (6), we substitute

$$\tilde{\omega} = \frac{I_2}{I_3}\tilde{\omega}_2 \equiv \frac{1 + h_1^2 h_2^2}{1 + h_1^2}\tilde{\omega}_2, \tag{7}$$

where I_2 is the moment of inertia around the intermediate principal axis and

$$\tilde{\omega}_2 = \frac{L}{I_2}. \tag{8}$$

For $h_1 = h_2 = h$, equation (6) then becomes

$$T_{\rm d} = D(h,h)\frac{(1+h^2)^3 4h^2\mu Q}{(1+h^4)^3 \rho D_{\rm m}^2 \tilde{\omega}_2^3}. \tag{9}$$

For a vast majority of objects in our tumbling asteroids sample, we detected only the strongest apparent angular frequency $\tilde{\omega}_{\rm obs} \equiv 2\pi/P_{\rm obs}$,

[5] The actual quantity measured in most asteroid observations is an effective diameter, i.e., a diameter corresponding to the asteroid cross-section. For the triaxial ellipsoid with $h = 0.7$, the average effective diameter measured at random aspect is almost equal to the mean diameter ($D_{\rm eff} \doteq 1.02 D_{\rm m}$); the difference is much smaller than the typical uncertainties of asteroid size measurements.

with the highest amplitude usually in its 2nd harmonic. Without a detailed knowledge of the actual spin state and moments of inertia, we use $\tilde{\omega}_{\rm obs}$ as a proxy for $\tilde{\omega}_2$. Our final formula for the damping time then becomes

$$T_{\rm d} = D(h,h)\frac{(1+h^2)^3 h^2 \mu Q P_{\rm obs}^3}{(1+h^4)^3 2\pi^3 \rho D_{\rm m}^2}. \tag{10}$$

For $h = 0.7$ and $D(h,h) = 20.4$ given above, and assuming $\mu = 10^9\,{\rm Pa}$, $Q = 100$ and $\rho = 2000\,{\rm kg\,m^{-3}}$ typical for asteroids (see Breiter et al., 2012; Harris, 1994), we get

$$T_{\rm d} = \frac{P_{\rm obs}^3}{C^3 D_{\rm m}^2}, \tag{11}$$

where C is a constant of 36 for $P_{\rm obs}$ in hours, $D_{\rm m}$ in kilometers, and $T_{\rm d}$ in Gy.

5.1.2 Sharma et al. (2005) theory

Sharma et al. (2005) found that the nutational damping time for a linear, anelastic ellipsoid of revolution is

$$T_{\rm d} = D_{\rm s}(h_{\rm s})\frac{\mu Q_{\rm s}}{\rho a^2 \tilde{\omega}^3}, \tag{12}$$

where $D_{\rm s}(h_{\rm s})$ is a shape parameter dependent on the body's axial ratio $h_{\rm s} \equiv c/a$. It is

$$D_{\rm s}(h_{\rm s}) = {\rm sign}(1-h_{\rm s})\frac{8\pi}{15}\int_{\theta_{\rm i}}^{\theta_{\rm f}} \frac{1}{\sin\theta(\tilde{E}_0 + \tilde{E}_2\cos 2\theta)}{\rm d}\theta, \tag{13}$$

where $\theta_{\rm i}$ is an initial precession angle, $\theta_{\rm f}$ is a minimum observable precession angle, and $\tilde{E}_0$ and $\tilde{E}_2$ are functions of $h_{\rm s}$ (see Sharma et al., 2005). The quality factor $Q_{\rm s}$ differs from Breiter et al.'s Q due to their different definitions of the reference energy. Breiter et al. (2012) discussed that it can be approximately re-calibrated as

$$Q_{\rm s} \approx \frac{Q}{2}. \tag{14}$$

Like for the Breiter et al. (2012) formula above, we adapt the Sharma et al.'s damping time calculation in the four points.

(1) In eq. (3), we substitute $a \equiv D_{\rm m}/(2h_{\rm s}^{1/3})$, for the reason explained in

point 1 of Sect. 5.1.1. The adapted eq. (12) is

$$T_\mathrm{d} = D_\mathrm{s}(h_\mathrm{s}) \frac{4 h_\mathrm{s}^{2/3} \mu Q_\mathrm{s}}{\rho D_\mathrm{m}^2 \tilde{\omega}^3}. \tag{15}$$

(2) We assume $h_\mathrm{s} = 0.6$ as default. An ellipsoid of revolution with this c/a ratio roughly corresponds to a triaxial ellipsoid with $b/a = c/b = 0.7$ that we took as default in Sect. 5.1.1.

(3) We use $D_\mathrm{s}(h_\mathrm{s}) = 35.9$ for $h_\mathrm{s} = 0.6$ that I. Sharma (personal communication) calculated for damping from $\theta_\mathrm{i} = 85°$ to $\theta_\mathrm{f} = 15°$. The reason for the choice of the lower limit is the same as in point 3 of Sect. 5.1.1. Like the Breiter et al.'s D, the value of D_s is rather sensitive to the actual lower limit on θ. Their theory gives a somewhat slower damping for high wobbling angles than Breiter et al. (2012); a value of $D_\mathrm{s}(h_\mathrm{s})$ for $h_\mathrm{s} = 0.6$ and damping from 45° to 15° is 23.8, i.e., less by a factor of 1.51 than the adopted value for damping from 85°.

(4) In eq. (15), we substitute

$$\tilde{\omega}' = \frac{\tilde{\omega} + \tilde{\omega}_2}{2} = \tilde{\omega} \left(\frac{1}{2} + \frac{1}{1 + h_\mathrm{s}^2} \right). \tag{16}$$

Equation (15) then becomes

$$T_\mathrm{d} = D_\mathrm{s}(h_\mathrm{s}) \left(\frac{1}{2} + \frac{1}{1 + h_\mathrm{s}^2} \right)^3 \frac{4 h_\mathrm{s}^{2/3} \mu Q_\mathrm{s}}{\rho D_\mathrm{m}^2 \tilde{\omega}'^3}. \tag{17}$$

Analogously to Sect. 5.1.1, we take $\tilde{\omega}_\mathrm{obs} \equiv 2\pi/P_\mathrm{obs}$ as a proxy for $\tilde{\omega}'$. Our final formula for the damping time then becomes

$$T_\mathrm{d} = D_\mathrm{s}(h_\mathrm{s}) \left(\frac{1}{2} + \frac{1}{1 + h_\mathrm{s}^2} \right)^3 \frac{h_\mathrm{s}^{2/3} \mu Q_\mathrm{s} P_\mathrm{obs}^3}{2\pi^3 \rho D_\mathrm{m}^2}. \tag{18}$$

For $h_\mathrm{s} = 0.6$ and $D_\mathrm{s}(h_\mathrm{s}) = 35.9$ given above, and assuming $\mu = 10^9\,\mathrm{Pa}$, $Q_\mathrm{s} = 50$ (corresponding to $Q \approx 100$ per eq. (14)) and $\rho = 2000\,\mathrm{kg\,m^{-3}}$ typical for asteroids (see above), we get

$$T_\mathrm{d} = \frac{P_\mathrm{obs}^3}{C^3 D_\mathrm{m}^2}, \tag{19}$$

where C is a constant of 33 for P_obs in hours, D_m in kilometers, and T_d in Gy.

Comparison of eqs. (11) and (19) indicates that the formulation by Sharma et al. (2005) gives a somewhat slower dissipation, though the difference is smaller than previously thought. Breiter et al. (2012) discuss these differences and track them to a slightly different definition of reference energy being dissipated, assumptions about internal structure of the body and inclusion of higher-order frequency over-tones in Breiter et al. (2012) as always advocated

by Efroimsky and his colleagues. Overall, however, the difference is small for the purpose of our application below.

Damping times calculated from the new models of tumbling are shorter by a factor of about 9 and 7, respectively, than the damping timescale τ calculated by Harris (1994) with the formula identical to eqs. (11) and (19), but with $C = 17$. However, we note that the estimated value of $\mu Q = 10^{11}$ Pa is hardly more than a guess. Only confrontation with observations will allow to calibrate the value of C.

5.2 Constraints from the PA/NPA rotators data

In Fig. 8, we plotted the lines of constant damping time calculated using eq. (11) for $T_\mathrm{d} = 4.5$, 0.45, 0.045, and 0.0045 Gy. Further, we plotted two lines/curves for the damping time equal to the main belt asteroid [6] lifetime (T_life). We use two formulations for the $T_\mathrm{life}(D_\mathrm{m})$ function: (1) $T_\mathrm{life} = K D_\mathrm{m}^{0.5}$, where $K \simeq 400$ Myr for the asteroid diameter D_m in kilometers (Farinella et al., 1998), and (2) $T_\mathrm{life}(D_\mathrm{m})$ from Bottke et al. (2005, Fig. 14). Finally, we plotted there a line for $T_\mathrm{d} = T_\mathrm{YORP}$, where the YORP timescale was taken from Čapek and Vokrouhlický (2004) and adjusted for asteroids starting with general orientations of their spin vectors as described in Pravec et al. (2008). Note that the T_d calculation assumes constant μQ factor (cf. implications of its possible dependence on asteroid diameter below).

The data reveal that tumblers predominate among asteroids with $T_\mathrm{d} \gtrsim 0.2$ Gy. A statistical uncertainty of this estimate due to the low number of data around the PA/NPA rotators transition is about a factor of 2, but there is a likely dominating uncertainty of T_d calculated from the rotation damping theory itself (such as the correct value of the quality factor Q and its possible frequency dependence), which we cannot estimate yet.

Perhaps the most interesting feature of the PA/NPA rotators distribution is that the "transition line" (the line below which tumblers predominate) follows rather closely a line of *constant* damping time. However, the excitation time from any of the proposed mechanisms is not constant with diameter, so we would expect a greater slope of the separation line. Why the PA/NPA rotators separation line should follow a line of constant damping time is unclear — it does not follow collisional lifetime, and it does not follow excitation time, or YORP time scale. And it does not even match "primordial" age (4.5 Gyr, or even 1 Gyr). We suspect that either there is a combination of two or more spin evolution mechanisms in play, or that μQ is not constant, but it decreases with asteroid size. Indeed, we can expect that the elastic modulus μ is size-dependant and weaker for smaller rubble piles. This size dependence of μ

[6] For near-Earth asteroids, which probably spent most of their life in the main belt, we use the estimated main belt asteroid lifetime as an approximation for their likely age as well.

should lead to a flattening (lower slope) of the transition line, opposing the effect of shorter collisional lifetime and shorter excitation times with decreasing size. Thus the fact that the transition line seems to follow constant $T_{\rm d}$ line may be just a lucky balance of the competing effects.

6 Conclusions

Our extensive photometric observations of Apophis allowed us to determine its tumbling spin state. Its knowledge will be important for predicting the possibility of the asteroid's impact in 2068; the retrograde rotation increases the impact probability as the estimated range of semimajor axis drift by the Yarkovsky effect contains values for the keyhole of resonant return leading to the impact on 2068 April 12. However, considering the uncertainties involved in modeling $\mathrm{d}a/\mathrm{d}t$, we expect that only a direct measure of the semimajor axis drift will fully resolve the matter. It may happen after further astrometric and radar observations in 2020–2021. Nevertheless, even if the Apophis impact probability still remains very small and it will likely drop to zero when the orbit determination is improved in 2021, the study of its spin state and of the population of slowly tumbling asteroids in general is important for understanding the asteroid spin evolution processes.

Acknowledgements

The work at Ondřejov and the Charles University Prague was supported by the Grant Agency of the Czech Republic, Grants P209/12/0229 and 209/10/0537, and by the Ministry of Education of the Czech Republic, Grant LG12001. A.G. was supported by the Slovak Grant Agency for Science VEGA, Grant 1/0670/13. A.W.H. was supported through the NEO Observations program of NASA, grant NNX13AP56G. Support for PROMPT has been provided by the National Science Foundation under awards CAREER-0449001, AAG-0707634, and MRI-0836187. TRAPPIST is a project funded by the Belgian Fund for Scientific Research (Fonds de la Recherche Scientifique, F.R.S FNRS) under grant FRFC 2.5.594.09.F, with the participation of the Swiss National Science Fundation (SNF). E.J. and M.G. are FNRS Research Associates, J.M. is Research Director FNRS. C.O. thanks the Belgian FNRS for funding her PhD thesis. Based on data collected with the Danish 1.54-m telescope at the ESO La Silla Observatory within the NEOSource project.

APPENDIX

A Transformation between asteroid-fixed and inertial coordinate systems

The orientation of a tumbling asteroid in the inertial frame is given by the equations of motion for the Euler angles ϕ, θ and ψ (see Kaasalainen, 2001). We use a following convention for the radius vector transformation from the asteroid (body-fixed) coordinate system to the ecliptic coordinate system:

$$\begin{pmatrix} x \\ y \\ z \end{pmatrix} = R_z(\lambda_L) R_y(90^\circ - \beta_L) R_z(\phi) R_x(\theta) R_z(\psi) \begin{pmatrix} x' \\ y' \\ z' \end{pmatrix}, \tag{A.1}$$

where (x', y', z') are the vector coordinates in the asteroid (body-fixed) system and (x, y, z) are its coordinates in the inertial ecliptic coordinate system. $R_i(\alpha)$ is the matrix of rotation by angle α about the i-axis in the positive direction, i.e.

$$R_z(\alpha) = \begin{pmatrix} \cos(\alpha) & -\sin(\alpha) & 0 \\ \sin(\alpha) & \cos(\alpha) & 0 \\ 0 & 0 & 1 \end{pmatrix}, R_x(\alpha) = \begin{pmatrix} 1 & 0 & 0 \\ 0 & \cos(\alpha) & -\sin(\alpha) \\ 0 & \sin(\alpha) & \cos(\alpha) \end{pmatrix},$$

$$R_y(\alpha) = \begin{pmatrix} \cos(\alpha) & 0 & \sin(\alpha) \\ 0 & 1 & 0 \\ -\sin(\alpha) & 0 & \cos(\alpha) \end{pmatrix}.$$

References

Binzel, R.P., 2009. Spectral properties and composition of potentially hazardous Asteroid (99942) Apophis. Icarus 200, 480–485.

Black, G.J., Nicholson, P.D., Bottke, W.F., Burns, J.A., 1999. On a possible rotation state of (433) Eros. Icarus 140, 239–242.

Bottke, W.F., et al., 2005. Linking the collisional history of the main asteroid belt to its dynamical excitation and depletion. Icarus 179, 63–94.

Bottke, W.F., Vokrouhlický, D., Rubincam, D.P., Nesvorný, D., 2006. The Yarkovsky and YORP effects: Implications for asteroid dynamics. Annu. Rev. Earth Planet. Sci. 34, 157–191.

Breiter, S., Rożek, A., Vokrouhlický, D., 2011. Yarkovsky-O'Keefe-Radzievskii-Paddack effect on tumbling objects. Mon. Not. R. Astron. Soc. 417, 2478–2499.

Breiter, S., Rożek, A., Vokrouhlický, D., 2012. Stress field and spin axis relaxation for inelastic triaxial ellipsoids. Mon. Not. R. Astron. Soc. 427, 755–769.

Burns, J.A., Safronov, V.S., 1973. Asteroid nutation angles. Mon. Not. R. Astron. Soc. 165, 403–411.

Čapek, D., Vokrouhlický, D., 2005. Accurate model for the Yarkovsky effect. In Knežević, Z., Milani, A. (Eds.) Proc. IAU Coll. 197, pp. 171–178.

Chesley, S.R., 2006. Potential impact detection for near-Earth asteroids: The case of 99942 Apophis (2004 MN4). In: Lazzaro, D., Ferraz-Mello, S., Fernndez, J. (Eds.), Asteroids, Comets, Meteors. Cambridge University Press, Cambridge, pp. 215-228.

Chesley, S.R., Milani, A., Tholen, D., Bernardi, F., Chodas, P., Micheli, M., 2009. An updated assessment of the impact threat from 99942 Apophis. DPS meeting 41, abstract 43.06.

Farinella, P., Vokrouhlický, D., Hartmann, W.K., 1998. Meteorite delivery via Yarkovsky orbital drift. Icarus 132, 378–387.

Farnocchia, D., et al., 2013. Yarkovsky-driven impact risk analysis for asteroid (99942) Apophis. Icarus 224, 192-200.

Giorgini, J.D., Benner, L.A.M., Ostro, S.J., Nolan, M.C., Busch, M.W., 2008. Predicting the Earth encounters of (99942) Apophis. Icarus 193, 1-19.

Hapke, B., 1993. Theory of reflectance and emittance spectroscopy. Cambridge Univ. Press, p. 346, equation (12.55).

Harris, A.W., 1994. Tumbling asteroids. Icarus 107, 209–211.

Henych, T., Pravec, P., 2013. Asteroid rotation excitation by subcatastrophic impacts. Mon. Not. R. Astron. Soc. 432, 1623–1631.

Hudson, R.S., Ostro, S.J., 1995. Shape and non–principal axis spin state of asteroid 4179 Toutatis. Science 270, 84–86.

Jehin, E., Gillon, M., Queloz, D., et al., 2011, The Messenger, 145, 2.

Kaasalainen, M., 2001. Interpretation of lightcurves of precessing asteroids. Astron. Astrophys. 376, 302–309.

Landolt, A.U., 1992. UBVRI photometric standard stars in the magnitude range 11.5-16.0 around the celestial equator. Astron. J. 104, 340–371, 436–491.

Mottola, S., et al., 1995. The slow rotation of 253 Mathilde. Planet. Space Sci.

43, 1609–1613.

Oey, J., 2010. Light curve analysis of asteroids from Leura and Kingsgrove Observatory in the first half of 2009. Minor Planet Bull. 37, 135–136.

Pravec, P., et al., 2005. Tumbling asteroids. Icarus 173, 108–131.

Pravec, P., et al., 2006. Photometric survey of binary near-Earth asteroids. Icarus 181, 63–93.

Pravec, P., et al., 2008. Spin rate distribution of small asteroids. Icarus 197, 497–504.

Samarasinha, N.H., A'Hearn, M.F., 1991. Observational and dynamical constraints on the rotation of Comet P/Halley. Icarus 93, 194–225.

Scheeres, D.J., 2001. Changes in rotational angular momentum due to gravitational interactions between two finite bodies. Celest. Mech. Dyn. Astron. 81, 39–44.

Scheeres, D.J., Ostro, S.J., Werner, R.A., Asphaug, E., Hudson, R.S., 2000. Effects of gravitational interactions on asteroid spin states. Icarus 147, 106-118.

Scheeres, D.J., et al., 2005. Abrupt alteration of Asteroid 2004 MN4's spin state during its 2029 Earth flyby. Icarus 178, 281–283.

Scheirich, P., et al., 2010. The shape and rotation of asteroid 2008 TC3. Meteoritics Planet. Sci. 45, 1804–1811.

Sharma, I., Burns, J.A., Hui, C.-Y., 2005. Nutational damping times in solids of revolution. Mon. Not. R. Astron. Soc. 359, 79–92.

Spencer, J.R., et al., 1995. The lightcurve of 4179 Toutatis: Evidence for complex rotation. Icarus 117, 71–89.

Vokrouhlický, D., 1998. Diurnal Yarkovsky effects for meter-sized asteroidal fragments' mobility: II. Non-sphericity effects. Astron. Astrophys. 338, 353–363.

Vokrouhlický, D., 1999. A complete linear model for the Yarkovsky thermal force on spherical asteroid fragments. Astron. Astrophys. 344, 362–366.

Vokrouhlický, D., Čapek, D., Chesley, S.R., Ostro, S.J., 2005. Yarkovsky detection opportunities. I. Solitary asteroids. Icarus 173, 166–184.

Vokrouhlický, D., Breiter, S., Nesvorný, D., Bottke, W.F., 2007. Icarus 191, 636–650.

Warner, B.D., 2007. Initial results from a dedicated H–G project. Minor Planet Bull. 34, 113–119.

Warner, B.D., Harris, A.W., Pravec, P., 2009. The asteroid lightcurve database. Icarus 202, 134–146.

Zappalà, V., Cellino, A., Barucci, A.M., Fulchignoni, M., Lupishko, D.F., 1990. An analysis of the amplitude-phase relationship among asteroids. Astron. Astrophys. 231, 548–560.

Table 1: Observational sessions

Date UT	R.A.	Decl.	d	r	α	Telescope
	[h m]	[° ′]	[AU]	[AU]	[°]	
2012-12-23.3	10 42	-27 22	0.102	1.000	77.6	Prompt 1
2012-12-25.3	10 33	-27 23	0.101	1.006	74.3	Prompt 1
2012-12-26.3	10 28	-27 23	0.101	1.009	72.7	Prompt 1
2012-12-27.2	10 23	-27 21	0.101	1.011	71.2	Prompt 1
2012-12-28.2	10 18	-27 19	0.100	1.014	69.5	Prompt 1
2012-12-29.2	10 13	-27 14	0.100	1.017	67.8	Prompt 1
2012-12-30.2	10 08	-27 10	0.099	1.019	66.2	Prompt 1
2012-12-31.2	10 03	-27 03	0.099	1.022	64.5	Prompt 1
2013-01-03.2	9 47	-26 34	0.098	1.029	59.5	Prompt 1
2013-01-04.2	9 41	-26 20	0.097	1.032	57.9	Prompt 1
2013-01-05.2	9 36	-26 06	0.097	1.034	56.2	Prompt 1
2013-01-06.1	9 30	-25 51	0.097	1.036	54.7	Pic du Midi 1-m
2013-01-06.2	9 30	-25 49	0.097	1.036	54.6	Prompt 1
2013-01-07.2	9 24	-25 30	0.097	1.039	52.9	Prompt 1
2013-01-07.6	9 22	-25 22	0.097	1.040	52.3	Leura 0.35-m
2013-01-08.1	9 19	-25 11	0.097	1.041	51.5	Danish 1.54-m
2013-01-08.1	9 19	-25 11	0.097	1.041	51.5	Pic du Midi 1-m
2013-01-08.2	9 18	-25 10	0.097	1.041	51.3	Prompt 1
2013-01-09.1	9 13	-24 49	0.097	1.043	49.9	Danish 1.54-m
2013-01-09.1	9 13	-24 49	0.097	1.043	49.9	Danish 1.54-m
2013-01-09.2	9 12	-24 46	0.097	1.043	49.7	Prompt 1
2013-01-09.3	9 12	-24 44	0.097	1.043	49.5	TRAPPIST 0.6-m
2013-01-10.1	9 07	-24 24	0.097	1.045	48.3	Danish 1.54-m
2013-01-10.2	9 06	-24 22	0.097	1.045	48.1	Prompt 1
2013-01-10.3	9 06	-24 19	0.097	1.046	48.0	TRAPPIST 0.6-m
2013-01-11.1	9 01	-23 57	0.097	1.047	46.7	Danish 1.54-m
2013-01-11.3	9 00	-23 52	0.097	1.048	46.4	Danish 1.54-m
2013-01-11.5	8 59	-23 46	0.097	1.048	46.1	Leura 0.35-m
2013-01-12.1	8 55	-23 28	0.097	1.049	45.2	Danish 1.54-m
2013-01-12.2	8 55	-23 25	0.097	1.050	45.1	Prompt 1
2013-01-12.2	8 55	-23 25	0.097	1.050	45.1	Danish 1.54-m
2013-01-13.1	8 49	-22 57	0.097	1.051	43.7	Danish 1.54-m
2013-01-13.2	8 49	-22 54	0.097	1.052	43.6	Prompt 1
2013-01-14.1	8 44	-22 24	0.097	1.053	42.3	Danish 1.54-m
2013-01-14.1	8 44	-22 24	0.097	1.053	42.3	Danish 1.54-m
2013-01-14.2	8 43	-22 20	0.097	1.054	42.2	Prompt 1
2013-01-15.1	8 38	-21 49	0.098	1.055	40.9	Danish 1.54-m
2013-01-15.2	8 37	-21 45	0.098	1.056	40.8	Prompt 1
2013-01-15.5	8 35	-21 34	0.098	1.056	40.4	Leura 0.35-m
2013-01-16.1	8 32	-21 12	0.098	1.057	39.6	Danish 1.54-m
2013-01-16.1	8 32	-21 12	0.098	1.057	39.6	Danish 1.54-m
2013-01-16.3	8 31	-21 04	0.098	1.058	39.4	Danish 1.54-m
2013-01-16.3	8 31	-21 04	0.098	1.058	39.4	Prompt 1
2013-01-19.1	8 15	-19 11	0.100	1.063	36.2	Danish 1.54-m
2013-01-19.2	8 15	-19 07	0.100	1.063	36.1	Prompt 1

Table 1: Observational sessions

Date UT	R.A.	Decl.	d	r	α	Telescope
	[h m]	[° ′]	[AU]	[AU]	[°]	
2013-01-20.1	8 10	-18 28	0.101	1.065	35.2	Danish 1.54-m
2013-01-20.2	8 10	-18 24	0.101	1.065	35.1	Prompt 1
2013-01-22.2	7 59	-16 54	0.103	1.068	33.5	Danish 1.54-m
2013-01-22.3	7 59	-16 50	0.103	1.068	33.5	Danish 1.54-m
2013-01-23.1	7 55	-16 13	0.104	1.070	33.0	Danish 1.54-m
2013-01-23.2	7 55	-16 08	0.104	1.070	32.9	Prompt 1
2013-01-24.1	7 50	-15 26	0.105	1.071	32.4	Danish 1.54-m
2013-01-24.2	7 50	-15 22	0.105	1.071	32.4	Prompt 1
2013-01-24.3	7 49	-15 17	0.105	1.072	32.4	Danish 1.54-m
2013-02-04.1	7 10	-6 46	0.123	1.086	33.8	Danish 1.54-m
2013-02-05.1	7 07	-6 01	0.125	1.087	34.4	Danish 1.54-m
2013-02-05.3	7 07	-5 53	0.126	1.087	34.5	Danish 1.54-m
2013-02-06.1	7 05	-5 17	0.128	1.088	35.0	Danish 1.54-m
2013-02-06.2	7 04	-5 13	0.128	1.088	35.1	Danish 1.54-m
2013-02-06.9	7 03	-4 43	0.129	1.089	35.5	Ondřejov 0.65-m
2013-02-07.1	7 02	-4 34	0.130	1.089	35.7	Danish 1.54-m
2013-02-07.2	7 02	-4 29	0.130	1.089	35.7	Danish 1.54-m
2013-02-08.1	7 00	-3 51	0.132	1.090	36.4	Danish 1.54-m
2013-02-08.2	7 00	-3 47	0.132	1.090	36.4	Danish 1.54-m
2013-02-12.1	6 53	-1 09	0.142	1.093	39.3	Danish 1.54-m
2013-02-13.1	6 52	-0 31	0.145	1.094	40.1	Danish 1.54-m
2013-02-13.2	6 52	-0 27	0.145	1.094	40.2	Danish 1.54-m
2013-02-14.2	6 50	0 10	0.148	1.094	40.9	Prompt 1
2013-02-14.2	6 50	0 10	0.148	1.094	40.9	Danish 1.54-m
2013-02-15.1	6 49	0 43	0.150	1.095	41.6	Danish 1.54-m
2013-02-15.1	6 49	0 43	0.150	1.095	41.6	Prompt 1
2013-02-16.0	6 48	1 15	0.152	1.095	42.3	Danish 1.54-m
2013-02-16.2	6 48	1 22	0.153	1.096	42.5	Danish 1.54-m
2013-02-16.2	6 48	1 22	0.153	1.096	42.5	Prompt 1
2013-02-17.0	6 48	1 49	0.155	1.096	43.0	Danish 1.54-m
2013-02-17.2	6 47	1 56	0.156	1.096	43.2	Danish 1.54-m
2013-02-17.2	6 47	1 56	0.156	1.096	43.2	Prompt 1
2013-02-18.0	6 47	2 23	0.158	1.096	43.8	Danish 1.54-m
2013-02-18.2	6 47	2 30	0.159	1.096	44.0	Prompt 1
2013-02-19.9	6 46	3 25	0.163	1.097	45.2	Pic du Midi 1-m
2013-03-09.1	6 49	10 38	0.215	1.096	56.3	Danish 1.54-m
2013-03-10.2	6 50	11 00	0.218	1.095	56.9	Danish 1.54-m
2013-03-11.0	6 51	11 15	0.221	1.095	57.3	Danish 1.54-m
2013-03-12.0	6 52	11 33	0.224	1.094	57.9	Danish 1.54-m
2013-03-13.0	6 53	11 51	0.227	1.094	58.4	Danish 1.54-m
2013-04-09.0	7 33	17 20	0.297	1.060	70.7	Danish 1.54-m
2013-04-12.0	7 38	17 43	0.303	1.054	71.9	Danish 1.54-m
2013-04-14.1	7 42	17 57	0.307	1.050	72.8	Danish 1.54-m
2013-04-15.0	7 44	18 03	0.308	1.048	73.2	Danish 1.54-m

Table 2
Parameters of the Apophis model with their estimated admissible uncertainties (corresponding to 3σ confidence level).

Fitted parameters:	
$\lambda_L(^\circ)$	250^a
$\beta_L(^\circ)$	-75
$\phi_0(^\circ)$	152^{+173}_{-64}
$\psi_0(^\circ)$	14^{+44}_{-11}
P_ψ (h)	263 ± 6
P_ϕ (h)	27.38 ± 0.07
$I_a \equiv I_1/I_3$	$0.61^{+0.11}_{-0.08}$
$I_b \equiv I_2/I_3$	$0.965^{+0.009}_{-0.015}$
Derived parameters:	
$(P_\phi^{-1} - P_\psi^{-1})^{-1} = P_1$ (h)	30.56 ± 0.01
$\theta_{\rm min}(^\circ)$	12 ± 4
$\theta_{\rm max}(^\circ)$	55^{+9}_{-20}
$\theta_{\rm aver}(^\circ)$	37^{+6}_{-14}
$a_{\rm dyn}/c_{\rm dyn}$	1.51 ± 0.18
$b_{\rm dyn}/c_{\rm dyn}$	1.06 ± 0.02
$a_{\rm shp}/c_{\rm shp}$	1.64 ± 0.09
$b_{\rm shp}/c_{\rm shp}$	$1.14^{+0.04}_{-0.08}$
E/E_0	1.024 ± 0.013

[a]The major and minor semiaxes of the uncertainty area of the direction of $\vec{L}$ are 27° and 14°, respectively, see Fig. 4.
The angles ϕ_0 and ψ_0 are for the epoch JD 2456284.676388 (= 2012 Dec. 23.176388 UT), light-travel time corrected (i.e., asterocentric).
E/E_0 is a ratio of the rotational kinetic energy and the lowest energy for given angular momentum, defined as $E_0 = L^2/(2I_3)$.